RSC Advances

ROYAL SOCIETY OF CHEMISTRY

www.rsc.org/advances

Table of Contents Graphic:

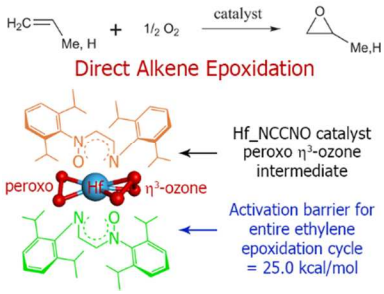

Direct alkene epoxidation catalytic cycles were computed for hafnium-based catalysts containing bis(dinitrone) and bis(imine nitrone) ligation using molecular oxygen as oxidant without co-reductant.

Hafnium Catalysts for Direct Alkene Epoxidation using Molecular Oxygen as Oxidant

Bo Yang and Thomas A. Manz*

Department of Chemical & Materials Engineering, New Mexico State University, Las Cruces, NM 88003-8001.

*corresponding author email: tmanz@nmsu.edu

Abstract:

New zirconium (Zr) based organometallic catalysts for direct olefin epoxidation using O_2 as oxidant without coreductant were introduced in a previous computational study (T. A. Manz and B. Yang, *RSC Advances*, 2014, **4**, 27755–27774). In this paper, we use density functional theory (DFT) to study three Hf-based catalysts with the same bis(bidentate) ligands as the preceding Zr-based catalysts: (a) the diimine ligand N(Ar)-CH-CH-N(Ar) aka NCCN, (b) the imine-nitrone ligand N(Ar)-CH-CH-N(Ar)-O aka NCCNO, and (c) the dinitrone ligand O-N(Ar)-CH-CH-N(Ar)-O aka ONCCNO [Ar = $-C_6H_3$-2,6-$^iPr_2$]. Complete reaction cycles and energetic spans (i.e., effective activation energies for the entire catalytic cycle) are computed for propene epoxidation. For Hf_NCCNO and Hf_ONCCNO, the reaction cycles are similar to the Zr-based analogs and the formation of η^3-ozone intermediates is still crucial. Hf_ONCCNO has a large enthalpic energetic span (60.4 kcal/mol) due to forming inert octahedral complexes as the catalyst resting state. Our calculations predict an energetic span ≥ 40 kcal/mol for Hf_NCCN, which indicates it will not be a good catalyst. Computed enthalpic energetic spans of ~30 kcal/mol are achieved for the Hf_NCCNO and Zr_NCCNO catalysts; however, transfer of allylic hydrogen from the reaction product forms a low energy deactivation product. Therefore, the Hf_NCCNO and Zr_NCCNO catalysts are only suitable for direct epoxidation of alkenes that do not have any allylic hydrogen atoms. As an example of an alkene with no allylic hydrogens, we computed enthalpic energetic spans (kcal/mol) for direct ethylene epoxidation of (a) 25.0 for Hf_NCCNO, (b) 30.2 for Zr_NCCNO, and (c) 52.7 for Zr_NCCN.

keywords: selective oxidation, alkene epoxidation, oxygen transfer reactions, propylene oxide, non-innocent ligands, redox-active ligands, Hf organometallic complexes, peroxide complexes, ethylene oxide, propene epoxidation, ethylene epoxidation, transition metal complexes

1. Introduction

Propylene oxide is an important chemical intermediate used to make polymers (polyurethanes, polyethers), oxygenated solvents (propylene glycol ethers), and industrial fluids (monopropylene glycol and polyglycol).[1, 2] Despite its importance, there is still no direct oxidation process that uses only propene and molecular oxygen (O_2) as reactants for industrial propylene oxide production.[1, 2] Propylene oxide is currently manufactured by the chlorohydrin, the co-oxidation, the cumene hydroperoxide, and the hydrogen peroxide processes. The chlorohydrin process produces enormous amounts of by-products in the form of salts and chlorinated organic molecules.[1, 2] The organic hydroperoxide process produces a co-product (usually styrene or *tert*-butyl alcohol), and the market value of this co-product strongly influences the process economics.[1, 2] The hydrogen peroxide (H_2O_2) process requires H_2 transportation and H_2O_2 on-site preparation and has the key advantage of producing mainly water as the co-product.[3-9] The cumene hydroperoxide process also consumes one equivalent of H_2 to produce mainly water as the co-product.[2, 10] There is intense interest in trying to make practical the direct epoxidation of propene with O_2 as oxidant without using a coreductant and without producing co-products or by-products.

To date, a large variety of heterogeneous catalysts were investigated for alkene epoxidation.[11-18] Particles of different metals as well as their binary combinations were deposited on various matrices and tested for direct propene epoxidation.[19, 20] However, for essentially all of these catalysts, the selectivity for propylene oxide is unsatisfactory.[19] The silver catalysts used for industrial direct ethene epoxidation exhibit low selectivity for propene epoxidation.[21, 22] However, Lei *et al.* showed subnanometer silver particles have good activity and selectivity for direct propene epoxidation.[23] Gold nanoparticles over various carriers (e.g., Au/TiO_2 and Au/TS-1) have attracted a lot of research.[24-30] At low conversions in the presence of H_2-containing feed, Au/TS-1 gave high selectivity (~90%) towards propylene oxide formation.[31] Copper has also been studied for direct propene epoxidation.[32, 33]

A large number of homogeneous catalysts are available to epoxidize alkenes, and many of these catalysts can use hydroperoxides as the oxidant.[11, 18, 34-44] High propylene oxide selectivities with acceptable propene conversions can be obtained when using hydroperoxides. However, very few homogeneous catalysts can use an oxygen molecule as the oxidant and nearly all of the ones that do require a coreductant to regenerate the catalyst after one of the oxygen

atoms has been transferred to the substrate.[39, 43] When a coreductant is used, only one of the oxygen atoms from molecular O_2 is utilized to form the desired product, with the other oxygen atom forming a by-product or co-product.

Uncatalyzed propene epoxidation has also been studied. Kizilkaya, et al. computationally studied a gas phase radical chain reaction using an oxygen molecule to produce propylene oxide; however, this process also produces oxygenated by-products.[45] Bach *et al.* computationally studied alkene epoxidation using peroxyformic acid as the oxidant, an activation barrier of 12–16 kcal/mol was computed, and this process produces an oxygenated co-product.[46]

Manz and Yang recently reported a new catalytic route for selective oxidation using molecular oxygen as the oxidant without requiring a coreductant.[47] This new catalytic cycle involves the formation of an η^3-ozone group that sequentially adds two O atoms to substrate molecules to form an oxo group that adsorbs an O_2 molecule to form an η^2-ozone group.[47] The η^2-ozone group rearranges to regenerate the η^3-ozone group.[47] Detailed reaction mechanisms and activation barriers for each step were computed for three Zr organometallic complexes.[47] Chemical potential diagrams were computed to study the relative stability of different catalyst forms as a function of oxygen chemical potential.[47] Since Hf is chemically similar to Zr, we study the three analogous Hf-based catalyst architectures for direct propene epoxidation in this article. These catalysts contain two bidentate ligands with (a) N(Ar)-CH-CH-N(Ar) (aka NCCN), (b) N(Ar)-CH-CH-N(Ar)-O (aka NCCNO), and (c) O-N(Ar)-CH-CH-N(Ar)-O (aka ONCCNO) linkages, where Ar= $-C_6H_3$-2,6-$^iPr_2$. The spiro bisperoxo states of these catalysts are shown in Figure 1.

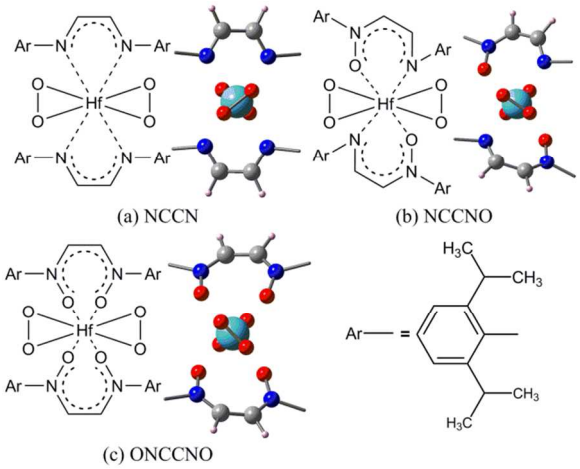

Figure 1: The spiro bisperoxo complexes of (a) Hf_NCCN which has bis(diimine) ligation, (b) Hf_NCCNO which has bis(imine-nitrone) ligation, and (c) Hf_ONCCNO which has bis(dinitrone) ligation. In the ball and stick molecular models, the Ar ligand portions are not shown for display proposes.

To the best of our knowledge, catalytic direct epoxidation of alkenes using molecular oxygen as the oxidant without coreductant has not been experimentally performed yet using any Zr- or Hf-based catalysts. Zr and Hf organometallic complexes have been used for alkene epoxidation using tert-butyl hydroperoxide as the oxidant.[34] Enantioselective epoxidation of homoallylic alcohols has been performed over chiral Zr catalysts using cumene hydroperoxide as the oxidant.[49] A Zr organometallic complex activated molecular oxygen that subsequently epoxidized an olefin group in a non-catalytic reaction in which the formed epoxide remained covalently bound to the metal and a methyl group on one of the ligands was irreversibly reduced to a methoxy group.[50, 51] Sulfated zirconia has been used as a promoter to enhance the epoxidation activity of titanosilicalite-1 (TS-1) using aqueous hydrogen peroxide as the oxidant.[52] Our work facilitates the catalytic transfer of both oxygen atoms from molecular O_2 to substrate molecules (e.g., alkene) to produce substrate oxide molecules (e.g., alkene oxide) without requiring a coreductant.

2. Methods

DFT calculations were carried out using GAUSSIAN software.[53] Becke's three-parameter hybrid method involving the Lee, Yang, and Parr correlation functional[54, 55] (B3LYP) and LANL2DZ basis sets[53] were chosen to achieve a good balance between accuracy and computational cost. The majority of previous DFT studies of organometallic and

polyoxometalate catalysts for olefin epoxidation also used the B3LYP functional.[15, 36, 38, 40, 41, 56-61] Therefore, our use of the B3LYP functional has the advantage of providing energies that can be readily compared to these previous computational studies. While the basis sets we used are not large, they provide adequate size and accuracy for studies to separate 'good' from 'bad' catalysts. In a previous paper, we found B3LYP/LANL2DZ optimized geometries to be in good agreement with experimental x-ray diffraction structures for two different forms of the Zr_NCCN catalyst.[47] The DFT computations described in this manuscript took approximately two hundred thousand computational hours to complete. Using similar methods, repeating these calculations with substantially larger basis sets would take on the order of one million computational hours.

For completeness, we studied both singlet and triplet geometries. For each reaction step, we considered various starting geometries and potential reaction pathways. All atoms of ground state reactants and products were fully relaxed during geometry optimization. Transition state geometries were optimized using the following procedure. First, constrained optimizations were performed along potential reaction coordinates to generate an initial transition state estimate. This transition state estimate was subsequently optimized using the quadratic synchronous transit (GAUSSIAN keyword QST3) or eigenmode following (GAUSSIAN keyword TS) methods. Both ground and transition state geometries were optimized to within 0.005 Å for the atom displacements and 0.0025 a.u. for the forces. In rare cases when geometry convergence was especially difficult, the geometry was considered converged when the root-mean-squared force was $< 10^{-4}$ a.u. Frequency analysis was performed on all optimized geometries. For each ground state geometry, we verified that all frequencies are real. For each transition state geometry, we verified that there is only one imaginary frequency (within a computational tolerance of 30 cm^{-1}). The imaginary frequency was animated in GaussView to verify the vibration was along the desired reaction pathway.

Thermochemical analysis was performed using the harmonic approximation (as implemented in GAUSSIAN 09) at a pressure of 1 atm and temperature of 298.15 K as the standard condition. The zero-point energy (E_{zp}), enthalpy (H, at standard condition), and Gibbs free energy (G, at standard condition) for all geometries we studied are reported in the Electronic Supplementary Information. For catalysts involving ions, such as for example Group 4 organometallic olefin polymerization catalysts, solvation effects play a key role in the reaction

kinetics by lowering the ion pair separation energy.[62-64] Since the catalysts studied here do not involve ions, the relative importance of solvation effects will be smaller. In this case, gas phase calculations (i.e., without solvent) provide sufficient accuracy to identify which catalysts are the most promising for experimental synthesis. Therefore, we did not include any solvation effects and all calculations were performed in the gas phase. We note that two DFT studies of Mo-based organometallic catalysts for olefin epoxidation showed negligible effects of aprotic solvation on the computed reaction energy profiles.[60, 65]

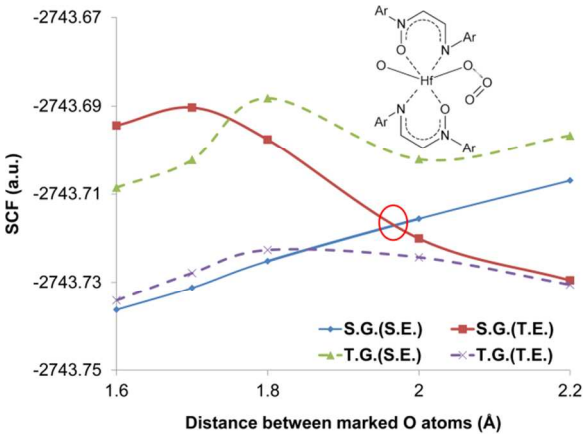

Figure 2: O_2 molecule adsorption on the Hf_NCCNO dioxo complex. The energy barrier for this step was estimated according to the singlet-triplet crossing point circled in red. Legend: S.G. = singlet geometry, S.E. = singlet energy, T.G. = triplet geometry, T.E. = triplet energy.

As indicated by the constrained geometry optimizations, there is no regular transition state for O_2 addition to the dioxo complex of each catalyst. Under this circumstance, the activation barrier was defined by the singlet-triplet crossing point where a vertical transition (i.e., at constant geometry) occurred. As demonstrated in Figure 2, the crossing point was located by a series of singlet and triplet constrained geometry optimizations, where the constrained coordinate was the distance between adjacent O atoms in the O_3 group. (The distance between the O atom that remains bound to Hf and the adjacent O atom that leaves to form O_2.) Because the singlet geometry curve properly describes the Hf-O bond at short O-O distances (while the triplet geometry curve does not), the crossing point occurs where the triplet energy at the singlet geometry equals the singlet energy at the singlet geometry. At this point, the total spin magnetic moment of the complex shifts between 0 and 2 (singlet and triplet). At O-O distances shorter than the crossing point value, the complex will prefer a singlet state and transform into an ozone

group. At O-O distances longer than the crossing point value, the complex will prefer a triplet state and transform into an oxo group plus free O_2 molecule. Similar plots for the Hf_NCCN and Hf_ONCCNO catalysts are shown in Figs. S1 and S7, respectively.

3. Results and Discussion

3.1. Chemical Potential Diagrams

To achieve direct propene epoxidation using only propene and O_2 as reactants, the catalyst should have several key properties. The catalyst should be able to react with O_2 molecules to form oxygenated organometallic complexes. The bonding strength between adjacent O atoms in the oxygenated organometallic complexes should be sufficiently weak to allow a propene molecule to react with and extract an O atom from the oxygenated organometallic complex. Since two O atoms are contributed by each O_2 molecule, the catalyst must be capable of sequentially transferring two O atoms to reactants.

Figure 3 shows three different bisperoxo conformations for the Hf catalyst: a) spiro structure ($M(O_2)_{2(spiro)}$), b) planar structure ($M(O_2)_{2(planar)}$), and c) butterfly structure ($M(O_2)_{2(butterfly)}$). In the spiro conformation, the two peroxo groups on opposite sides of the Hf atom are almost perpendicular to each other. In the planar conformation, the two peroxo groups are almost coplanar with each other and the Hf atom. In the butterfly conformation, the two peroxo groups are lifted up like wings from the metal.

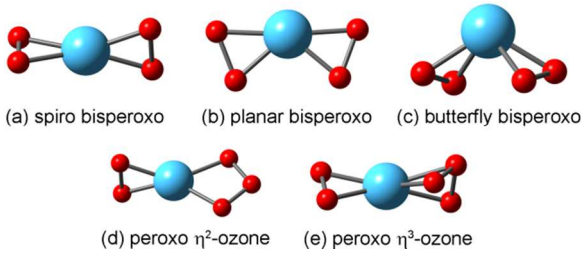

Figure 3: Three different bisperoxo conformations: (a) spiro, (b) planar, and (c) butterfly. Two different peroxo ozone conformations: (d) peroxo η^2-ozone and (e) peroxo η^3-ozone. (blue: Hf, red: O) Ligands are included in the calculations but are not presented here for display purposes.

As shown in Figure 3 (d) and (e), ozone groups can bond to the metal center via two (i.e., η^2-ozone) or three (i.e., η^3-ozone) oxygen atoms. The dihedral angle between O(outer)-O(μ)-O(outer') and O(outer)-Hf-O(outer') was used to distinguish η^2-ozone from η^3-ozone, where O(outer) and O(outer') are the two outer O atoms in the ozone group and O(μ) is the central atom in the ozone group. Specifically, η^2-ozone complexation corresponded to a dihedral angle > 135°, while a dihedral angle < 135° implied η^3-ozone complexation. The η^3-ozone group is the

key feature that makes direct propene epoxidation possible. Since the μ-O atom in η^3-ozone forms a (partial) bond to the Hf atom, it is already in the position that when one of the outer oxygen atoms is removed by propene, the μ-O atom along with the other remaining oxygen atom can readily form a peroxo group. In contrast, none of the O atoms from the η^2-ozone group can be easily removed by a propene molecule.

Due to thermal collisions, different catalyst forms can exist at the same time within one reactor and transform between each other. Catalyst forms with lower energy tend to be more stable. Chemical potential diagrams (Figure 4 (Hf_NCCNO), Fig. S2 (Hf_NCCN), and Fig. S8 (Hf_ONCCNO)) were computed to study the relative energies of different catalyst forms as a function of oxygen chemical potential. In these diagrams, the x-axis plots the oxygen chemical potential. The chemical potential of an O atom in the O_2 molecule is taken as the reference state of 0 kcal/mol. On this scale, the chemical potential of an O atom in propylene oxide (aka PO) is -15.94 kcal/mol, which corresponds to the computed reaction energy for P + ½ O_2 → PO. In each chemical potential diagram, the y-axis plots the relative energy for each catalyst form compared to the singlet spiro bisperoxo complex. On the oxygen-rich side (i.e., at the oxygen chemical potential of O_2), the relative energy for each structure (S) was calculated by the formula:

$$E_S + \frac{N}{2} \cdot E_{O_2} - E_{\text{bisperoxo}}.$$

On the oxygen-starved side (i.e., at the oxygen chemical potential of PO), the relative energy for each structure (S) was calculated by the formula:

$$E_S + N \cdot (E_{\text{propylene oxide}} - E_{\text{propene}}) - E_{\text{bisperoxo}}.$$

Here, N is the difference of oxygen atom number between structure (S) and the bisperoxo complex. E_S represents the electronic energy of structure S without zero point vibrations or thermal contributions (aka SCF energy).

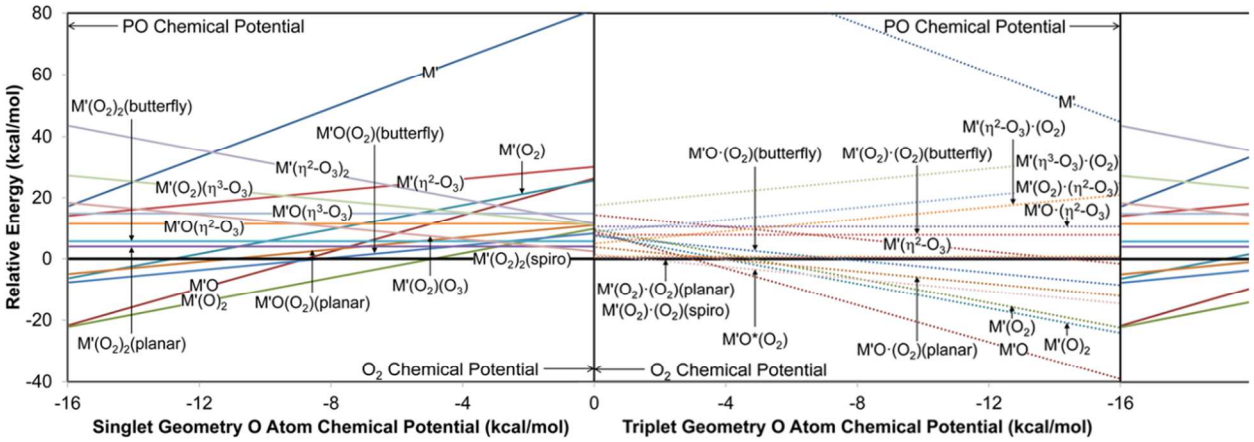

Figure 4: Computed chemical potential diagram for Hf_NCCNO catalyst. The Hf_NCCNO singlet spiro bisperoxo complex ($M'(O_2)_{2(spiro)}^{S}$) is the reference state. Subscripts in parentheses indicate the catalyst conformation.

For convenience, we use the notation M'' to represent the Hf/Zr_NCCN catalyst, M' to represent the Hf/Zr_NCCNO catalyst, and M to represent the Hf/Zr_ONCCNO catalyst. (O) represents an oxo group. (O_2) represents a peroxo or weakly adsorbed O_2 group, (η^2-O_3) and (η^3-O_3) represents η^2- and η^3-ozone groups, respectively. "·" indicates a weakly adsorbed oxygen group and "*" indicates an even more weakly adsorbed oxygen group. Subscript numbers show the quantity of corresponding oxygen groups and the subscripts in parentheses indicate different geometric conformations. For these chemical potential diagrams, singlet geometries and energies are shown in the left panel and triplet geometries and energies are shown in the middle panel. The right panel is a partial copy of the left panel to enable direct comparison of singlet and triplet energies. In the following reaction cycles, tables, and discussion, a superscript T indicates a triplet state and a superscript S indicates a singlet state.

Figure 4 shows the computed chemical potential diagram for the Hf_NCCNO catalyst. The bare complex, M', has the highest relative energy (81.1 kcal/mol) on the oxygen-rich end, indicating that M' easily adsorbs O_2 to form oxygenated forms. The bis-η^2-ozone complex ($M'(\eta^2\text{-}O_3)_2$) has the highest relative energy (43.4 kcal/mol) on the oxygen-starved end. Therefore, the bis-η^2-ozone complex will not be stable and would easily react with propene to form propylene oxide. On the oxygen-rich end, all the major catalyst forms containing from one to six adsorbed oxygen atoms settle within a ~25 kcal/mol window. This suggests the complex should work great as an oxygen transfer catalyst.

Atomic spin moments (ASMs) of selected triplet states are listed in Tables S1 (Hf_NCCN), S3 (Hf_NCCNO), and S6 (Hf_ONCCNO) to quantify the spin density distribution among atoms. ASMs were computed using the Density Derived Electrostatic and Chemical method.[66, 67] Each catalyst has been divided into several parts: metal, strongly adsorbed O atoms, weakly adsorbed O atoms, N atoms in ligand 1, N atoms in ligand 2, and the remainder of the structure. Results are tabulated by adding ASMs for all atoms in the respective part. In each table, ligand 1 is arbitrarily designated as the ligand having larger ASMs for nitrogen atoms. The combined ASMs for all parts sum to 2.00, representing the two unpaired electrons. Except for the bare complexes, the Hf atoms in all structures have small ASMs in the range from -0.11 to +0.11. In general, a large portion of the spin density (ASMs of ~1) reside on weakly adsorbed non-ligand oxygen atoms. Ligand nitrogen atoms are the second dominant parts for occupying the spin. In all of the structures except the dioxo complexes, the strongly adsorbed O atoms hold little spin.

3.2. Computed reaction cycles

Catalytic cycles with transition states and energies were computed. We use the term 'master cycle' to refer to a catalytic cycle comprised of two or more junior cycles. Optimized ground and transition state geometries were calculated using the B3LYP/LANL2DZ level of theory in GAUSSIAN software as described in Section 2 above. Figure 5 shows the Hf_NCCNO master cycle containing three junior cycles. Transition states involving propylene oxide formation are illustrated in greater detail in Figure 6.

The singlet junior cycle on the right-hand side of Figure 5 involves oxidized forms ranging from three to five adsorbed oxygen atoms in addition to the ligand O atoms. Specifically, the spiro bisperoxo complex ($M'(O_2)_{2(spiro)}{}^{S}$) reacts with propene to form propylene oxide and the oxo peroxo complex ($M'O(O_2)_{(planar)}{}^{S}$). This oxo peroxo complex adsorbs one oxygen molecule to form the peroxo η^2-ozone complex ($M'(O_2)(\eta^2\text{-}O_3)^{S}$). The peroxo η^2-ozone complex transforms into the peroxo η^3-ozone complex ($M'(O_2)(\eta^3\text{-}O_3)^{S}$) with a small energy change. The peroxo η^3-ozone complex reacts with propene to give out another propylene oxide and regenerate $M'(O_2)_{2(spiro)}{}^{S}$ to finish one whole cycle. As mentioned in Section 3.1, the Hf_NCCNO system contains several bisperoxo complexes. The spiro bisperoxo complex has the lowest energy among all three conformations and plays an important role in the reaction kinetics.

Planar and butterfly conformations are energetically unfavorable and would transform into the spiro conformation.

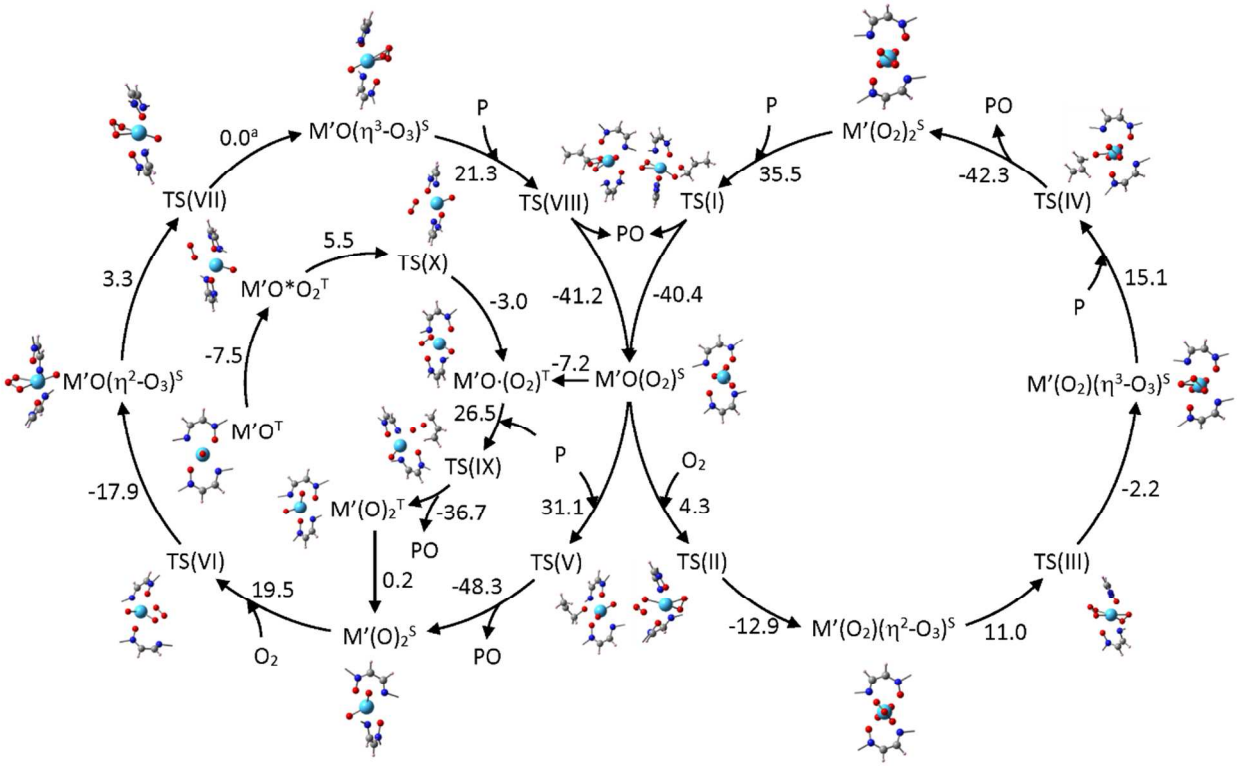

Figure 5: Master catalytic cycle for direct propene epoxidation using Hf_NCCNO catalyst. Energy differences are presented in kcal/mol. P and PO represent propene and propylene oxide, respectively. [a]Within a computational precision of ~0.1 kcal/mol, the energy difference between M'O(η^3-O_3)^S and TS(VII) is negligible. In the displayed chemical structures, portions of the ligands are unillustrated for display purposes.

The other singlet junior cycle involves oxidized forms ranging from two to four oxygen atoms in addition to the ligand O atoms. Specifically, the oxo peroxo complex (M'O$(O_2)_{(planar)}^S$) reacts with propene to form propylene oxide and the dioxo complex (M'$(O)_2^S$). The dioxo complex and one oxygen molecule react to form the oxo η^2-ozone complex (M'(O)(η^2-O_3)^S). The oxo η^2-ozone complex transforms into the oxo η^3-ozone complex (M'(O)(η^3-O_3)^S) with a small energy change. The oxo η^3-ozone complex reacts with propene to give out another propylene oxide and regenerate M'O$(O_2)_{(planar)}^S$ to finish one whole cycle.

As shown in Figure 5, there is a detour through triplet states that substantially lowers the overall energy barrier for this catalyst. Specifically, the M'O$(O_2)_{(planar)}^S$ transforms into M'O·$(O_2)_{(planar)}^T$ and releases 7.2 kcal/mol of energy. This process is followed by propene

addition to produce propylene oxide plus $M'(O)_2^T$, which would eventually transform into the $M'(O)_2^S$. Alternatively, $M'O\cdot(O_2)_{(planar)}^T$ can be generated from $M'O^T$ via an exothermic reaction passing through $M'O^*(O_2)^T$. There is no transition barrier from MO^T to $MO^*(O_2)^T$. The activation barrier for propylene oxide formation over $M'O\cdot(O_2)_{(planar)}^T$ is 26.5 kcal/mol compared to 31.1 kcal/mol over $M'O(O_2)_{(planar)}^S$.

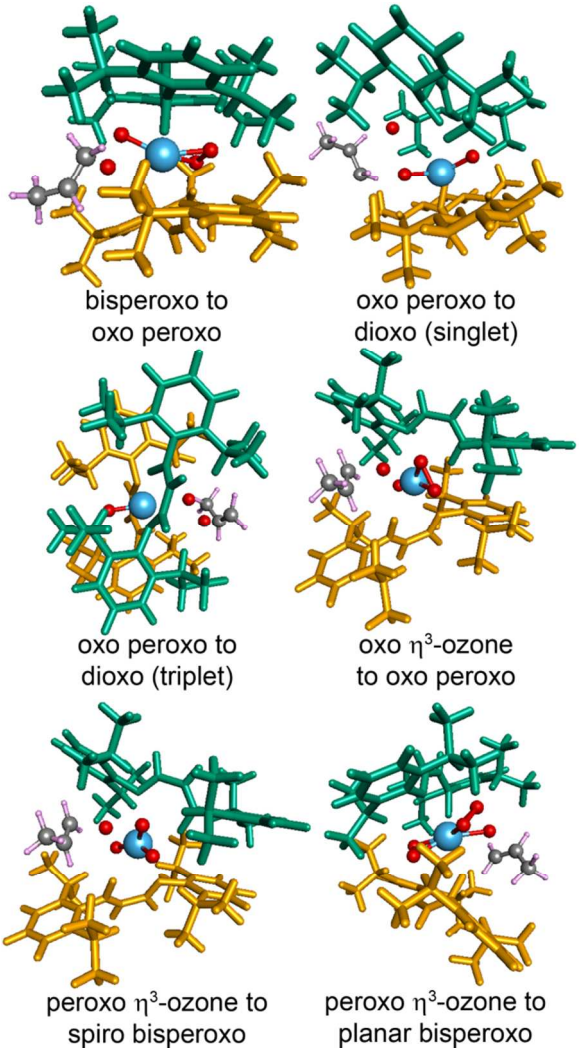

Figure 6: Transition states for forming propylene oxide over the Hf_NCCNO catalyst. Ligands colored orange and green. Other atoms: C (gray), H (small pink), O (red), Hf (cyan).

Fig. S9 shows the Hf_ONCCNO master cycle containing three junior cycles for direct propene epoxidation. Comparing Fig. S9 to Figure 5, master catalytic cycles for the Hf_NCCNO and Hf_ONCCNO systems are similar. However, the octahedral complex ($M(O)_{2(oct)}^T$) in the Hf_ONCCNO system has the lowest relative energy (Fig. S8) and forms a dormant catalyst

resting state that destroys the catalyst performance. The SCF reaction energy for forming $M(O)_2^S$ from $M(O)_{2(oct)}^T$ is 32.7 kcal/mol, and this leads to a large SCF energetic span of 57.2 kcal/mol (see ESI for details). Therefore, the Hf_NCCNO system is a better choice for direct alkene epoxidation.

3.3. Potential catalyst deformation and interconversion processes

One possible deformation process happens when an oxo group reacts with an oxygen molecule. Normally the reaction of an oxygen molecule with an oxo group is expected to produce a η^2-ozone group. However, the oxygen molecule can also attack the oxo group in such a way that one O atom from O_2 becomes attached to the oxo atom and the other O atom from O_2 attacks the ligand C=C bond (instead of the Hf metal). This forms a heterocyclic ring containing the metal center and the ligand. Example structures and computed energies can be found in Figs S53 and S93. Since the energies of such cyclized structures are higher (10.4 and 0.8 kcal/mol for the Hf_NCCNO and Hf_ONCCNO systems) than the corresponding η^2-ozone intermediates, the ligand cyclization products would be unstable with respect to other catalyst forms. Therefore, the ligand cyclization reactions are kinetically unimportant.

Table 1: Energies (kcal/mol) relative to the singlet spiro bisperoxo complexes[a]

Ligand	Deformation product(s)	Abbrev.	E	E_{ZP}	H	G
NCCN	O insertion into ligand	NCOCN	-24.1	-22.1	-22.6	-16.9
NCCNO	O inserts to break ligand	ON+OCCN	-9.1	-9.6	-10.3	-2.8
ONCCNO	O inserts to break ligand	ON+OCCNO	-10.9	-10.6	-11.0	-3.6
ONCCNO	singlet octahedral complex	$M(O)_{2(oct)}^S$	-21.0	-22.3	-22.1	-32.8
ONCCNO	triplet octahedral complex	$M(O)_{2(oct)}^T$	-27.8	-30.5	-30.7	-43.2

[a] The O atom chemical potential was taken to be that of molecular O_2.

In another possible deformation process, an oxygen atom can potentially attack the C=C group in the ligand backbone of all three catalysts (Figure 7 (a), (b) and (c)). Our DFT calculations started with epoxide-like geometry guesses where an oxygen atom bonds to both carbon atoms in the C=C group. However, geometries converged to other structures indicating epoxide formation is unfavorable. The Hf_NCCN system formed an ether-like geometry in which the oxygen atom inserted between the two ligand carbon atoms to produce a NCOCN linkage. We call this a deformation product rather than a deactivation product, because we do not

know whether the resulting structure would have higher or lower direct alkene epoxidation activity than the starting structure. For the Hf_NCCNO and Hf_ONCCNO systems, a different kind of deformation reaction was observed in which the ligand was split into two pieces with one of the C–N bonds broken by the oxygen atom. Energies for each of these deformation products relative to the spiro bisperoxo complexes are given in Table 1. Although these deformation products have lower energies than the spiro bisperoxo complexes, we expect the activation barriers for forming these deformation products would be high, because they split C-C or C-N bonds.

Another deformation process involves oxygen attacking a ligand C atom to form the octahedral complex ($M(O)_{2(oct)}$), as shown in Figure 7(d). In contrast to ligand cyclization, the attacking oxygen comes from an oxo group bound to Hf. $M(O)_{2(oct)}^{T}$ is the catalyst resting state. This kind of deformation process has only been revealed in the bis(dinitrone) catalysts (i.e., Hf_ONCCNO and Zr_ONCCNO) and does not occur for the Hf_NCCN and Hf_NCCNO systems.

Table 2: Energies (kcal/mol) of triplet octahedral complexes involving allylic H transfer. For reactants and products, the listed energies are relative to PO desorption to form the triplet oxo complex. For each transition state, the listed energy is relative to the corresponding reactant.

Metal	Ligand	Structure	Figure	E	E_{ZP}	H	G
Hf	NCCNO	reactant	S60	0.0	-0.8	-0.1	11.0
Hf	NCCNO	transition state	S146	7.5	7.2	6.1	9.6
Hf	NCCNO	product	S61	-59.2	-59.0	-58.5	-46.1
Hf	ONCCNO	reactant	7e, S102	-2.7	-1.2	-1.1	14.1
Hf	ONCCNO	transition state	S159	4.4	2.6	1.9	3.8
Hf	ONCCNO	product	7f, S103	-51.7	-51.5	-50.8	-38.7
Zr	NCCNO	reactant	S163	1.9	1.2	1.9	14.3
Zr	NCCNO	transition state	S165	8.2	8.0	6.8	10.9
Zr	NCCNO	product	S164	-51.9	-51.5	-51.1	-37.5

However, for both the NCCNO and ONCCNO ligands another kind of octahedral complex can form when the alkene and alkene oxide contain one or more allylic hydrogen atoms. For this kind of deformation process, the reactant consists of an alkene oxide molecule adsorbed on the MO^{T} complex (ONCCNO ligand, Figure 7(e)) or an alkene molecule chemisorbed on the $M'(O)_2^{T}$ complex (NCCNO ligand). The deformation product is a triplet octahedral complex in which one allylic hydrogen atom has been transferred to form an OH group bound to the metal

(Figure 7(f)). The transition state for this deformation reaction was computed for the Hf_ONCCNO, Hf_NCCNO, and Zr_NCCNO catalysts. Energetic results are summarized in Table 2. Because the activation barriers for allylic hydrogen transfer are low, we expect this reaction to occur fast. The product in which the allylic hydrogen is transferred to form a metal-bound OH group has extremely low energy (about 50 kcal/mol lower in energy than PO desorption). Unfortunately, therefore, alkenes with allylic hydrogens will undergo this side reaction involving allylic hydrogen transfer. Future work should focus on using these catalysts for direct epoxidation of alkenes without allylic hydrogens or modifying the catalyst structure to prevent this unwanted allylic hydrogen transfer.

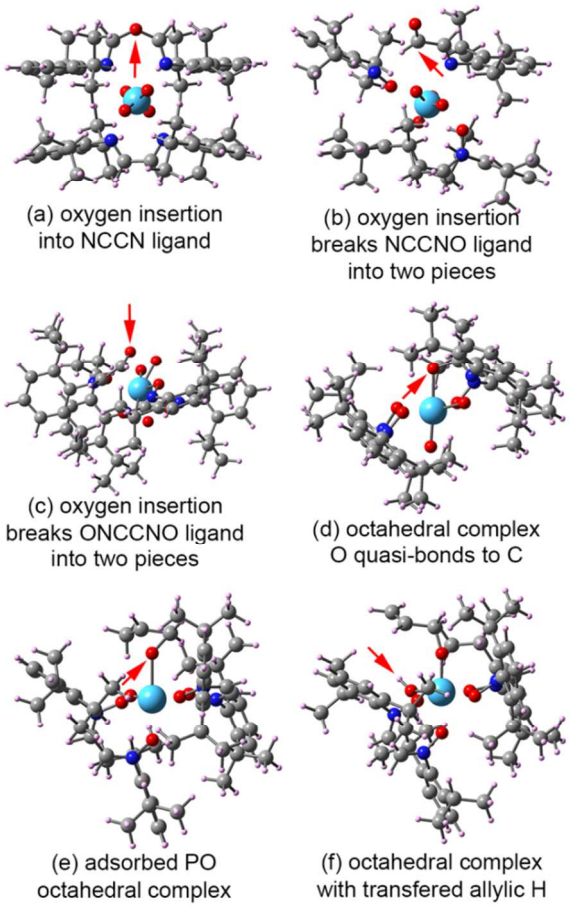

Figure 7: Possible deformation products. Red arrows indicate reaction sites.

The NCCN, NCCNO, and ONCCNO ligands could potentially interconvert by reacting the ligand N atom with an O atom. Table 3 summarizes the ligand interconversion energies for the spiro bisperoxo complexes under different oxygen conditions. The oxygen-rich condition uses an O_2 molecule as the oxygen atom source. The oxygen-starved condition uses a PO

molecule as the oxygen atom source. However, we expect very high activation barriers for propene to rip an O atom off the ligands, because adequate space is not readily available for propene to attack ligand O atoms. Under oxygen-rich conditions, the M"$(O_2)_{2(spiro)}^S$ complex is ~30 kcal/mol higher in energy than the M$(O_2)_{2(spiro)}^S$ complex, and the M'$(O_2)_{2(spiro)}^S$ is ~10 kcal/mol higher in energy than the M$(O_2)_{2(spiro)}^S$ complex. However, the calculated free energies show smaller differences. The M'$(O_2)_{2(spiro)}^S$ complex is only 0.9 kcal/mol higher in free energy than the M$(O_2)_{2(spiro)}^S$ complex, and the M"$(O_2)_{2(spiro)}^S$ complex is only 10 kcal/mol higher in free energy than the M$(O_2)_{2(spiro)}^S$ complex. "Ligand interconversion appears to be a slow process under normal conditions. For example, Stanciu et al.[73] reported the crystal structure of M"$(O_2)_{2(spiro)}$ but did not mention any ligand interconversion even though the complex was observed for several days."[47]

Table 3: Energies (kcal/mol) of different ligation relative to the ONCCNO spiro bisperoxo complex (M$(O_2)_{2(spiro)}^S$). Data for oxygen-rich and oxygen-starved (in parentheses) conditions are presented.

complex	notation	E	E_{ZP}	H	G
NCCN spiro bisperoxo	M"$(O_2)_{2(spiro)}^S$	32.1 (-31.7)	27.1 (-27.6)	28.1 (-29.8)	10.4 (-22.7)
NCCNO spiro bisperoxo	M'$(O_2)_{2(spiro)}^S$	13.0 (-18.8)	10.1 (-17.2)	10.8 (-18.2)	0.9 (-15.7)
ONCCNO spiro bisperoxo	M$(O_2)_{2(spiro)}^S$	0.0 (0.0)	0.0 (0.0)	0.0 (0.0)	0.0 (0.0)

3.4. Energetic spans

Energetic spans were computed for each catalyst based on the SCF energy, E_{ZP}, enthalpy, and Gibbs free energy. As reviewed by Kozuch and Shaik, the energetic span permits kinetic assessment of computationally calculated catalytic cycles.[48] To calculate the energetic span, the turnover-determining intermediate (TDI) and turnover-determining transition state (TDTS) need to be identified. To compute the TDI and TDTS, first we construct reaction cycle(s) containing the catalyst resting state(s) under reaction conditions. Chemical potential diagrams, such as those presented in Section 3.1, are helpful in identifying the catalyst resting state(s) under reaction conditions. After constructing catalytic cycle(s) containing the catalyst resting state(s), the next step is to imagine the catalytic cycle as a wheel with an arbitrary starting point. The TDI is that intermediate, which if chosen as the starting point of the catalytic cycle, results in the highest

subsequent energy barrier along one complete forward cycle that returns to the intermediate, and the state producing this energy barrier is called the TDTS. The energetic span is the energy difference from the TDI to the TDTS along the forward direction of the catalytic cycle. If the master cycle contains multiple junior cycles, this process is repeated for each junior cycle containing the catalyst resting state(s). In this case, the energetic span is the minimum value for all junior cycles containing the catalyst resting state(s). Importantly, this whole process is performed independently for each energy type (i.e., E, E_{ZP}, H, and G), and the TDI and TDTS may be different for each energy type. The enthalpic energetic span is an estimate of the effective activation barrier for the entire catalytic cycle.[48]

Table 4 summarizes the computed thermodynamic data and energetic spans for the Hf_NCCNO system. As the chemical potential diagram in Figure 4 shows, $M'O^T$ is the low energy form (and therefore catalyst resting state) over the majority of oxygen chemical potential range. $M'O^T$ can weakly adsorb O_2 to form $M'O^*(O_2)^T$ which rearranges to form $M'O\cdot(O_2)_{(planar)}{}^T$. Epoxidation occurs first when a propene reacts with $M'O\cdot(O_2)_{(planar)}{}^T$ and gives out $M'(O)_2{}^T$ and propylene oxide as products. $M'(O)_2{}^T$ would form an equilibrium with $M'(O)_2{}^S$ and the latter can follow the oxo η^3-ozone cycle: $M'(O)_2{}^S \rightarrow M'O(\eta^2\text{-}O_3)^S \rightarrow M'O(\eta^3\text{-}O_3)^S \rightarrow M'O(O_2)_{(planar)}{}^S \rightarrow M'O\cdot(O_2)_{(planar)}{}^T$. The forward barrier for this oxo η^3-ozone cycle is maximized at 26.6 kcal/mol with $M'(O)_2{}^T$ as TDI and TS(VIII) as TDTS. Comparing the thermodynamic data of the Hf_NCCNO system with the Zr_NCCNO system that we reported previously, half of the reaction barriers are slightly higher in the Hf_NCCNO system and the other half are slightly lower. Reaction steps with higher activation barriers for Hf_NCCNO are TS(I) [4.8], TS(III) [1.6], TS(IV) [1.0], TS(VII) [0.9] and TS(VIII) [0.4] with energy differences in square brackets are presented in kcal/mol. Reaction steps with lower activation barriers for Hf_NCCNO are TS(II) [-10.4], TS(V) [-7.8], TS(VI) [-2.6], TS(X) [-2.0] and TS(IX) [-1.9]. The computed enthalpic energetic span for direct propene epoxidation over Hf_NCCNO is 30.0 kcal/mol, which is 0.5 kcal/mol higher than for the Zr_NCCNO catalyst. When the allylic H transfer deformation route is included, the SCF energy required to generate $M'(O)^T$ is 59.2 kcal/mol (Table 2). In this case, the transferred allylic H product (Fig. S61) is the TDI and TS(IX) is the TDTS leading to an SCF energetic span of 59.2-7.5+5.5-3.0+26.5=80.7 kcal/mol. This clearly demonstrates the key role of allylic H transfer in increasing the energetic span. As

shown in Table 4, allylic H transfer similarly increases the energetic span for the Zr_NCCNO catalyst.

These results indicate Hf_NCCNO may be a suitable catalyst for direct epoxidation of alkenes that do not have any allylic hydrogens. As an example of an alkene that does not contain any allylic hydrogen atoms, the master cycle for direct ethylene epoxidation using molecular O_2 as the oxidant over this catalyst is presented in Fig. S5. The form of this master cycle is analogous to that for direct propene epoxidation. Table S4 summarizes the corresponding reaction energies and energetic spans. The allylic hydrogen transfer by-product cannot be formed, because ethylene does not have any allylic hydrogens. This results in an enthalpic energetic span of only 25.0 kcal/mol for direct ethylene epoxidation over the Hf_NCCNO catalyst. In general, a "potentially promising" direct alkene epoxidation catalyst should have a computed enthalpic energetic span < 30 kcal/mol. (This number is based on the observation that most reactions that are facile over organometallic catalysts at near-ambient conditions have activation barriers less than ~30 kcal/mol.[68-72]) Based on these results and observations, the Hf_NCCNO system should be a good catalyst for direct ethylene epoxidation using molecular O_2 as the oxidant without coreductant.

Table 4: Computed reaction energies and energetic spans (kcal/mol) for the NCCNO ligand architecture

reactant	product	activation barrier				net rxn energy			
		E	E_{ZP}	H	G	E	E_{ZP}	H	G
$M'(O_2)_{2(spiro)}^{S}$+P	$M'O(O_2)_{(planar)}^{S}$+PO	35.5	35.9	35.6	48.9	-4.9	-3.7	-4.1	-4.1
$M'O(O_2)_{(planar)}^{S}$+O_2	$M'(O_2)(\eta^2\text{-}O_3)^{S}$	4.3	5.8	4.9	17.8	-8.6	-6.4	-7.0	4.5
$M'(O_2)(\eta^2\text{-}O_3)^{S}$	$M'(O_2)(\eta^3\text{-}O_3)^{S}$	11.0	10.3	9.9	10.9	8.8	8.5	8.3	8.9
$M'(O_2)(\eta^3\text{-}O_3)^{S}$+P	$M'(O_2)_{2(spiro)}^{S}$+PO	15.1	15.9	15.8	29.1	-27.2	-25.8	-26.1	-25.9
$M'O(O_2)_{(planar)}^{S}$+P	$M'(O)_2^{S}$+PO	31.1	31.3	31.2	44.3	-17.1	-7.2	-7.5	-7.3
$M'(O)_2^{S}$+O_2	$M'O(\eta^2\text{-}O_3)^{S}$	19.5	11.4	10.9	21.4	1.7	-5.3	-5.8	4.3
$M'O(\eta^2\text{-}O_3)^{S}$	$M'O(\eta^3\text{-}O_3)^{S}$	3.3[a]	3.5[a]	2.7[a]	6.7	3.3[a]	3.5[a]	2.7[a]	5.8
$M'O(\eta^3\text{-}O_3)^{S}$+P	$M'O(O_2)_{(planar)}^{S}$+PO	21.3	22.5	22.1	35.5	-19.8	-18.5	-19.1	-19.4
$M'O^{T}$+O_2	$M'O^*(O_2)^{T}$	0.0	0.0	0.0	4.5	-7.5	-6.1	-6.3	4.5
$M'O^*(O_2)^{T}$	$M'O\cdot(O_2)_{(planar)}^{T}$	5.5	5.1	4.8	5.7	2.5	3.1	2.8	4.0
$M'O\cdot(O_2)_{(planar)}^{T}$+P	$M'(O)_2^{T}$+PO	26.5	27.0	26.3	39.4	-10.2	-10.4	-10.6	-12.3
$M'(O)_2^{T}$	$M'(O)_2^{S}$	—	—	—	—	0.2	10.7	10.2	12.5
$M'O(O_2)_{(planar)}^{S}$	$M'O\cdot(O_2)_{(planar)}^{T}$	—	—	—	—	-7.2	-7.4	-7.2	-7.6

E_{span}	26.6	31.5	30.0	58.2
with allylic H transfer	80.7	82.9	81.3	93.9
E_{span} (Zr)	28.4	30.5[b]	29.5[b]	54.6[b]
with allylic H transfer (Zr)	73.7	76.2	74.6	87.6

[a] For this reaction, the potential energy surface between the transition state and reaction product is nearly flat—the transition state and reaction product have the same energy within the resolution of the calculation. [b] These results correct an error appearing in reference 47: the TDI and TDTS are M'O·$(O_2)_{(planar)}^T$ and TS(IX) for E_{SCF} and M'$(O)_2^S$ and TS(VIII) for E_{ZP}, H, and G, while results reported in reference 47 erroneously used M'O·$(O_2)_{(planar)}^T$ and TS(IX) as the TDI and TDTS for E_{ZP}, H, and G.

Table S7 summarizes the computed thermodynamic data and energetic spans for direct propene epoxidation over the Hf_ONCCNO catalyst. When including the allylic H transfer side reaction, the energetic spans are 70.1 (E), 73.7 (E_{ZP}), 71.4 (H), and 88.7 (G) kcal/mol. When omitting the allylic H transfer side reaction, the energetic spans are 57.2 (E), 60.6 (E_{ZP}), 60.4 (H), and 87.1 (G) kcal/mol. This system has too high energetic spans to be a practical direct alkene epoxidation catalyst. As shown in Table S7, the Zr_ONCCNO system exhibits similarly high energetic spans.

Finally, we note that M(η^3-O_3)·$(O_2)^T$, M'(η^3-O_3)·$(O_2)^T$, and M"(η^3-O_3)·$(O_2)^T$ junior cycles may potentially exist, but were not computed for all three Hf-based catalysts. As shown in Figure 4, the M'(η^3-O_3)·$(O_2)^T$ complex is higher in energy than the M'(O_2)(η^3-O_3)^S complex. Therefore, it is unlikely that considering the M'(η^3-O_3)·$(O_2)^T$ junior cycle would have lowered the energetic spans for the Hf_NCCNO catalyst. Because M''$(O_2)_{(spiro)}^S$ is the resting state of the Hf_NCCN catalyst and is also the TDI and reactant for the TDTS, considering the M"(η^3-O_3)·$(O_2)^T$ junior cycle could not have lowered the energetic span for the Hf_NCCN catalyst below 39.5 (E), 38.6 (E_{ZP}), 39.2 (H), and 47.8 (G) kcal/mol. As shown in Fig. S8, the M(η^3-O_3)·$(O_2)^T$ is similar in energy to M(O_2)(η^3-O_3)^S. Therefore, given the propensity of the Hf_ONCCNO catalyst to form inert octahedral complexes, considering the M(η^3-O_3)·$(O_2)^T$ junior cycle would not alter our overall conclusions that this catalyst is undesirable due to the formation of inert octahedral complexes.

3.5. Comparison between Zr-based and Hf-based catalysts

Zirconium and hafnium occur in the same chemical group and have similar chemical properties. In the Earth's crust, Zr occurs with an abundance of 1.65×10^{-4} kg/kg, and Hf occurs with an abundance of 3×10^{-6} kg/kg.[74] Because Hf is mined as a trace component of Zr minerals, Hf is more rare and expensive than Zr. Therefore, if a catalyst comprised of Hf performs similar

to an analogous Zr catalyst, the Zr-based catalyst will normally be preferred for economic reasons.

Similarities and differences between the Zr-based and Hf-based catalysts are now summarized. Direct propene epoxidation over the Zr_NCCN, Zr_NCCNO, and Zr_ONCCNO catalysts was described in our earlier report.[47] Energetics, reaction mechanisms, and geometric structures are nearly the same for the Zr_ONCCNO and Hf_ONCCNO systems. The only major difference is that the Hf_ONCCNO bare complex is ~25 kcal/mol more stable than the spiro bisperoxo complex on the oxygen-starved side (i.e., at the PO chemical potential), while the Zr_ONCCNO bare complex is higher in energy than the spiro bisperoxo complex across the entire chemical potential range. The Zr_NCCNO and Hf_NCCNO systems have similar energetics, reaction mechanisms, and geometric structures in all respects. The key difference between the Zr_NCCN and Hf_NCCN systems is that the singlet oxo η^3-ozone complex exists for the Zr_NCCN system but not for the Hf_NCCN system. The SCF activation barrier for reacting propene with the spiro bisperoxo complex to produce propylene oxide plus the singlet oxo peroxo complex is lowered from 54.3 kcal/mol for the Zr_NCCN system to 39.5 kcal/mol for the Hf_NCCN system. However, this SCF activation barrier of 39.5 kcal/mol for the Hf_NCCN system is still high enough to prevent the Hf_NCCN system from being a good catalyst.

We now present direct ethylene epoxidation results for Zr_NCCN and Zr_NCCNO. Fig. S4 (computed catalytic cycle) and Table S2 (reaction energies and energetic spans) summarize direct ethylene epoxidation calculations for Zr_NCCN. The direct ethylene epoxidation catalytic cycle and computed enthalpic energetic span of 52.7 kcal/mol are similar to our previously reported results[47] for direct propene epoxidation over Zr_NCCN. Fig. S6 (computed catalytic cycle) and Table S5 (reaction energies and energetic spans) summarize direct ethylene epoxidation calculations for Zr_NCCNO. These results are similar to those for Hf_NCCNO, except the computed enthalpic energetic span of 30.2 kcal/mol for Zr_NCCNO is higher than that of 25.0 kcal/mol for Hf_NCCNO.

4. Conclusions

In this article, we used DFT computations to study three Hf organometallic catalysts for direct alkene epoxidation using molecular oxygen as the oxidant without coreductant. The following types of bis(bidentate) ligation were studied: (a) bis(dinitrone) (e.g., O-N(Ar)-CH-CH-

N(Ar)-O), (b) bis(imine-nitrone) (e.g., N(Ar)-CH-CH-N(Ar)-O), and (c) bis(diimine) (e.g., N(Ar)-CH-CH-N(Ar)) where Ar = -C_6H_3-2,6-$^{i}Pr_2$. Analogous to the Zr catalysts, the formation of η^3-ozone intermediates is the crucial step in the catalytic cycle. In general, the catalytic cycle involves: (a) a peroxo or adsorbed O_2 group releases an O atom to substrate to form alkene oxide and an oxo group, (b) an oxygen molecule adds to the oxo group to generate an η^2-ozone group, (c) the η^2-ozone group rearranges to form an η^3-ozone group, (d) the η^3-ozone group releases an O atom to substrate to form alkene oxide and regenerate the peroxo group.

Direct propene epoxidation cycles were computed for the Hf_ONCCNO and Hf_NCCNO catalysts. These catalytic cycles are analogous to those for previously studied Zr catalysts by the same authors.[47] Among the three Hf catalysts investigated, Hf_NCCNO gave the lowest computed enthalpic energetic span (30.0 kcal/mol); however, transfer of allylic hydrogen from the reaction product forms a low energy deactivation product. Therefore, the Hf_NCCNO and Zr_NCCNO catalysts are only suitable for direct epoxidation of alkenes that do not have any allylic hydrogens. The computed enthalpic energetic span for Hf_ONCCNO is 60.4 kcal/mol compared to 57.9 kcal/mol for the Zr analog. These high energetic spans are due to the formation of inert octahedral complexes that make Hf_ONCCNO and Zr_ONCCNO unsuitable catalysts for alkene epoxidation. For Hf_NCCN, we determined the energetic span is $\geq$ 40 kcal/mol, which indicates it will not be a good catalyst. In summary, our computations showed the Hf catalysts were chemically similar to their Zr counterparts.

Direct ethylene epoxidation is easier than direct propene epoxidation, because ethylene does not have any allylic hydrogen atoms that could form allylic hydrogen transfer by-products. We computed catalytic cycles and the following energetic spans (kcal/mol) for direct ethylene epoxidation using molecular O_2 as the oxidant without co-reductant: (a) 25.0 for Hf_NCCNO, (b) 30.2 for Zr_NCCNO, and (c) 52.7 for Zr_NCCN. These results indicate Hf_NCCNO and Zr_NCCNO would make good catalysts for direct ethylene epoxidation, while Zr_NCCN would not.

Finally, we wish to make a few remarks about possibilities for further study. In a previous paper[47] as well as this one, our computations showed that Zr and Hf organometallic complexes may catalyze a new type of selective oxidation route that passes through η^3-ozone intermediates. This naturally leads to the question: "Can other transition metals besides Zr and Hf be used to construct selective oxidation catalysts passing through η^3-ozone intermediates?"

Because Ti, Zr, and Hf all belong to Group 4, it seems likely that Ti could also be used as the basis to construct such catalysts. Bearing in mind the smaller radius of a Ti atom compared to Zr and Hf, it seems likely that less sterically demanding ligands would be required to construct functional Ti analogs. Moreover, we envision the possibility that transition metals from other chemical groups (e.g., Groups 5–8) might also be able to catalyze selective oxidation processes passing through η^3-ozone intermediates. Further study should shed light on this issue.

When the alkene has one or more allylic hydrogen atoms, future studies should explore strategies for eliminating the allylic hydrogen transfer reaction. As described in Section 3.3 above, a dioxo-like complex facilitates allylic hydrogen transfer. Therefore, we recommend designing a new catalyst architecture M''' that stabilizes the following catalytic cycle: (a) M'''O + O_2 → M'''(η^2-O_3), (b) M'''(η^2-O_3) → M'''(η^3-O_3), (c) M'''(η^3-O_3) + P → M'''(O_2) + PO, (d) M'''(O_2) + P → M'''O + PO. Because this catalytic cycle does not involve the dioxo complex, M'''$(O)_2$, it may be able to avoid the allylic hydrogen transfer reaction. Therefore, computational screening studies should be performed to identify catalyst architectures that stabilize the M'''(η^3-O_3) form and destabilize the M'''$(O)_2$ form.

Another important topic for future research pertains to the catalyst phase. The complexes we described here, as well as in the previous article,[47] are homogeneous catalysts that would exist in the solution phase. For some reaction processes, it would be preferable to have a heterogeneous catalyst to facilitate catalyst separation from the reaction products. Therefore, the potential catalytic applications would increase if the catalyst could also be made in heterogeneous form. A recent article by Shylesh *et al.* reviews techniques for the heterogenization of complexes for single-site epoxidation catalysis.[16] Similar techniques could potentially be used to tether our organometallic complexes to a support, thereby providing heterogenized forms.

Acknowledgements: Supercomputing resources were provided by the Extreme Science and Engineering Discovery Environment (XSEDE). XSEDE is funded by NSF grant OCI-1053575. XSEDE project grants TG-CTS100027 and TG-CHE140142 provided allocations on the Trestles cluster at the San Diego Supercomputing Center (SDSC), the Stampede cluster at the Texas Advanced Computing Center (TACC), and the Steele cluster at Purdue University. The authors sincerely thank the technical support staff of XSEDE, SDSC, TACC, and Information

Technology at Purdue (ITaP). The authors and NMSU's Office of Intellectual Property (Arrowhead Center, Inc.) have applied for a patent on some of the results described in this paper.

Electronic supplementary information (ESI) available: DFT-optimized geometries and energies; imaginary frequency for each transition state; singlet-triplet crossing curves for O_2 addition to Hf_ONCCNO and Hf_NCCN dioxo complexes; constrained optimization curves showing oxo η^3-ozone and peroxo η^3-ozone complexes do not exist for the Hf_NCCN system; chemical potential diagrams for Hf_ONCCNO and Hf_NCCN; assigned spin magnetic moments tables; master cycle and table of reaction energies and energetic spans for direct propene epoxidation catalyzed by Hf_ONCCNO; master cycles and tables of reaction energies and energetic spans for direct ethylene epoxidation catalyzed by Zr_NCCN, Hf_NCCNO, and Zr_NCCNO.

5. References

1. D. Kahlich, U. Wiechern and J. Linder, in *Ullmann's Encyclopedia of Industrial Chemistry*, Wiley-VCH Verlag GmbH & Co. KGaA, Weinheim, Germany, 2012, vol. 30, pp. 313-335.
2. T. A. Nijhuis, M. Makkee, J. A. Moulijn and B. M. Weckhuysen, *Ind. Eng. Chem. Res.*, 2006, **45**, 3447-3459.
3. G. Blanco-Brieva, M. C. Capel-Sanchez, M. P. de Frutos, A. Padilla-Polo, J. M. Campos-Martin and J. L. G. Fierro, *Ind. Eng. Chem. Res.*, 2008, **47**, 8011-8015.
4. G. Grigoropoulou, J. H. Clark and J. A. Elings, *Green Chem.*, 2003, **5**, 1-7.
5. J. L. Zhao, J. C. Zhou, J. Su, H. C. Guo, X. S. Wang and W. M. Gong, *AIChE J.*, 2007, **53**, 3204-3209.
6. K. Kamata, K. Yonehara, Y. Sumida, K. Yamaguchi, S. Hikichi and N. Mizuno, *Science*, 2003, **300**, 964-966.
7. M. Ghanta, D. R. Fahey, D. H. Busch and B. Subramaniam, *ACS Sustainable Chem. Eng.*, 2013, **1**, 268-277.
8. X. Zuwei, Z. Ning, S. Yu and L. Kunlan, *Science*, 2001, **292**, 1139-1141.
9. H. J. Lee, T. P. Shi, D. H. Busch and B. Subramaniam, *Chem. Eng. Sci.*, 2007, **62**, 7282-7289.
10. T. Seo and J. Tsuji, Process for producing propylene oxide. U.S. Patent No. 6646139, Sumitomo Corporation, 2003.
11. Q. H. Xia, H. Q. Ge, C. P. Ye, Z. M. Liu and K. X. Su, *Chem. Rev.*, 2005, **105**, 1603-1662.
12. F. Cavani, *J. Chem. Technol. Biotechnol.*, 2010, **85**, 1175-1183.

13. B. F. Sels, D. E. DeVos and P. A. Jacobs, *Tetrahedron Lett.*, 1996, **37**, 8557-8560.
14. S. B. Shin and D. Chadwick, *Ind. Eng. Chem. Res.*, 2010, **49**, 8125-8134.
15. N. S. Antonova, J. J. Carbo, U. Kortz, O. A. Kholdeeva and J. M. Poblet, *J. Am. Chem. Soc.*, 2010, **132**, 7488-7497.
16. S. Shylesh, M. J. Jia and W. R. Thiel, *Euro. J. Inorg. Chem.*, 2010, **2010**, 4395-4410.
17. Y. Liu, K. Murata and M. Inaba, *Chem.Lett.*, 2006, **35**, 436-437.
18. B. S. Lane and K. Burgess, *Chem. Rev.*, 2003, **103**, 2457-2473.
19. M. Kahn, A. Seubsai, I. Onal and S. Senkan, *Top. Catal.*, 2010, **53**, 86-91.
20. I. Onal, D. Duzenli, A. Seubsai, M. Kahn, E. Seker and S. Senkan, *Top. Catal.*, 2010, **53**, 92-99.
21. M. A. Barteau and R. J. Madix, *J. Am. Chem. Soc.*, 1983, **105**, 344-349.
22. J. Q. Lu, J. J. Bravo-Suarez, A. Takahashi, M. Haruta and S. T. Oyama, *J. Catal.*, 2005, **232**, 85-95.
23. Y. Lei, F. Mehmood, S. Lee, J. Greeley, B. Lee, S. Seifert, R. E. Winans, J. W. Elam, R. J. Meyer, P. C. Redfern, D. Teschner, R. Schlogl, M. J. Pellin, L. A. Curtiss and S. Vajda, *Science*, 2010, **328**, 224-228.
24. J. Q. Chen, S. J. A. Halin, J. C. Schouten and T. A. Nijhuis, *Faraday Discuss.*, 2011, **152**, 321-336.
25. T. A. Nijhuis, J. Chen, S. M. A. Kriescher and J. C. Schouten, *Ind. Eng. Chem. Res.*, 2010, **49**, 10479-10485.
26. A. Pulido, M. Boronat and A. Corma, *J. Phys. Chem. C*, 2012, **116**, 19355-19362.
27. M. Sasidharan, A. K. Patra, Y. Kiyozumi and A. Bhaumik, *Chem. Eng. Sci.*, 2012, **75**, 250-255.
28. E. E. Stangland, K. B. Stavens, R. P. Andres and W. N. Delgass, *J. Catal.*, 2000, **191**, 332-347.
29. A. M. Joshi, W. N. Delgass and K. T. Thomson, *J. Phys. Chem. C*, 2007, **111**, 7841-7844.
30. T. Hayashi, K. Tanaka and M. Haruta, *J. Catal.*, 1998, **178**, 566-575.
31. B. Chowdhury, J. J. Bravo-Suarez, N. Mimura, J. Q. Lu, K. K. Bando, S. Tsubota and M. Haruta, *J. Phys. Chem. B*, 2006, **110**, 22995-22999.
32. H. Chu, L. Yang, Q. H. Zhang and Y. Wang, *J. Catal.*, 2006, **241**, 225-228.
33. L. J. Yang, J. L. He, Q. H. Zhang and Y. Wang, *J. Catal.*, 2010, **276**, 76-84.
34. K. A. Jorgensen, *Chem. Rev.*, 1989, **89**, 431-458.
35. J. M. Mitchell and N. S. Finney, *J. Am. Chem. Soc.*, 2001, **123**, 862-869.
36. E. M. McGarrigle and D. G. Gilheany, *Chem. Rev.*, 2005, **105**, 1563-1602.
37. J. T. Groves and T. E. Nemo, *J. Am. Chem. Soc.*, 1983, **105**, 5786-5791.
38. D. V. Deubel, G. Frenking, P. Gisdakis, W. A. Herrmann, N. Rosch and J. Sundermeyer, *Acc. Chem. Res.*, 2004, **37**, 645-652.
39. J. T. Groves and R. Quinn, *J. Am. Chem. Soc.*, 1985, **107**, 5790-5792.
40. P. Brandt, P. O. Norrby, A. M. Daly and D. G. Gilheany, *Chem. Eur. J.*, 2002, **8**, 4299-4307.
41. A. Comas-Vives, A. Lledos and R. Poli, *Chem. Eur. J.*, 2010, **16**, 2147-2158.
42. D. Steinborn, in *Fundamentals of Organometallic Catalysis*, Wiley-VCH Verlag & Co. KGaA, Weinheim, Germany, 2012, pp. 306-318.
43. H. Adolfsson and D. Balan, in *Aziridines and Epoxides in Organic Synthesis*, ed. A. K. Yudin, Wiley-VCH, Weinheim, Germany, 2006, pp. 185-228.

44. C. Dinoi, M. Ciclosi, E. Manoury, L. Maron, L. Perrin and R. Poli, *Chem. Eur. J.*, 2010, **16**, 9572-9584.
45. A. C. Kizilkaya, M. F. Fellah and I. Onal, *Chem. Phys. Lett.*, 2010, **487**, 183-189.
46. R. D. Bach, M. N. Glukhovtsev and C. Gonzalez, *J. Am. Chem. Soc.*, 1998, **120**, 9902-9910.
47. T. A. Manz and B. Yang, *RSC Adv.*, 2014, **4**, 27755-27774.
48. S. Kozuch and S. Shaik, *Acc. Chem. Res.*, 2011, **44**, 101-110.
49. T. Okachi, N. Murai and M. Onaka, *Org. Lett.*, 2003, **5**, 85-87.
50. T. V. Lubben and P. T. Wolczanski, *J. Am. Chem. Soc.*, 1985, **107**, 701-703.
51. T. V. Lubben and P. T. Wolczanski, *J. Am. Chem. Soc.*, 1987, **109**, 424-435.
52. D. Prasetyoko, Z. Ramli, S. Endud and H. Nur, *React. Kinet. Catal. Lett.*, 2005, **86**, 83-89.
53. M. J. Frisch, G. W. Trucks, H. B. Schlegel, G. E. Scuseria, M. A. Robb, J. R. Cheeseman, G. Scalmani, V. Barone, B. Mennucci, G. A. Petersson, H. Nakatsuji, M. Caricato, X. Li, H. P. Hratchian, A. F. Izmaylov, J. Bloino, G. Zheng, J. L. Sonnenberg, M. Hada, M. Ehara, K. Toyota, R. Fukuda, J. Hasegawa, M. Ishida, T. Nakajima, Y. Honda, O. Kitao, H. Nakai, T. Vreven, J. A. J. Montgomery, J. E. Peralta, F. Ogliaro, M. Bearpark, J. J. Heyd, E. Brothers, K. N. Kudin, V. N. Staroverov, T. Keith, R. Kobayashi, J. Normand, K. Raghavachari, A. Rendell, J. C. Burant, S. S. Iyengar, J. Tomasi, M. Cossi, N. Rega, J. M. Millam, M. Klene, J. E. Knox, J. B. Cross, V. Bakken, C. Adamo, J. Jaramillo, R. Gomperts, R. E. Stratmann, O. Yazyev, A. J. Austin, R. Cammi, C. Pomelli, J. W. Ochterski, R. L. Martin, K. Morokuma, V. G. Zakrzewski, G. A. Voth, P. Salvador, J. J. Dannenberg, S. Dapprich, A. D. Daniels, O. Farkas, J. B. Foresman, J. V. Ortiz, J. Cioslowski and D. J. Fox, Gaussian, Inc., Wallingford CT, 2010, GAUSSIAN 09 Revision C.01.
54. A. D. Becke, *J. Chem. Phys.*, 1993, **98**, 5648-5652.
55. P. J. Stephens, F. J. Devlin, C. F. Chabalowski and M. J. Frisch, *J. Phys. Chem.*, 1994, **98**, 11623-11627.
56. D. V. Deubel, J. Sundermeyer and G. Frenking, *J. Am. Chem. Soc.*, 2000, **122**, 10101-10108.
57. M. Herbert, F. Montilla, E. Alvarez and A. Galindo, *Dalton Trans.*, 2012, **41**, 6942-6956.
58. M. L. Kuznetsov and J. C. Pessoa, *Dalton Trans.*, 2009, **38**, 5460-5468.
59. I. Washington and K. Houk, *J. Am.Chem. Soc.*, 2000, **122**, 2948-2949.
60. P. Costa, M. Calhorda and F. Kuhn, *Organometallics*, 2010, **29**, 303-311.
61. P. Gisdakis, I. V. Yudanov and N. Rosch, *Inorg. Chem.*, 2001, **40**, 3755-3765.
62. T. A. Manz, K. Phomphrai, G. Medvedev, B. B. Krishnamurthy, S. Sharma, J. Haq, K. A. Novstrup, K. T. Thomson, W. N. Delgass, J. M. Caruthers and M. M. Abu-Omar, *J. Am. Chem. Soc.*, 2007, **129**, 3776-3777.
63. T. A. Manz, S. Sharma, K. Phomphrai, K. A. Novstrup, A. E. Fenwick, P. E. Fanwick, G. A. Medvedev, M. M. Abu-Omar, W. N. Delgass, K. T. Thomson and J. M. Caruthers, *Organometallics*, 2008, **27**, 5504-5520.
64. E. Y. X. Chen and T. J. Marks, *Chem. Rev.*, 2000, **100**, 1391-1434.
65. M. Herbert, F. Montilla and A. Galindo, *J. Mol.Catal. A: Chem.*, 2011, **338**, 111-120.
66. T. A. Manz and D. S. Sholl, *J. Chem. Theory Comput.*, 2012, **8**, 2844-2867.
67. T. A. Manz and D. S. Sholl, *J. Chem. Theory Comput.*, 2011, **7**, 4146-4164.

68. T. A. Manz, *QSARs for Olefin Polymerization Catalyzed by Ti and Zr Complexes*, Scholars' Press, Saarbrucken, Germany, 2013, pp. 1-310.
69. T. Manz, J. Caruthers, S. Sharma, K. Phomphrai, K. Thomson, W. Delgass and M. Abu-Omar, *Organometallics*, 2012, **31**, 602-618.
70. K. Lam, Z. Lin and T. Marder, *Organometallics*, 2007, **26**, 3149-3156.
71. J. W. Nelson, L. M. Grundy, Y. Dang, Z.-X. Wang and X. Wang, *Organometallics*, 2014, **33**, 4290-4294.
72. F. Jutz, A. Buchard, M. Kember, S. Fredriksen and C. Williams, *J. Am. Chem. Soc.*, 2011, **133**, 17395-17405.
73. C. Stanciu, M. E. Jones, P. E. Fanwick and M. M. Abu-Omar, *J. Am. Chem. Soc.*, 2007, **129**, 12400-12401.
74. D. R. Lide, ed., *CRC Handbook of Chemistry and Physics*, 87th edn., 2006, p. **14-**17.